PHYSICAL REVIEW B **83**, 155308 (2011)

Coherent population trapping in intersubband photocurrent spectra

Marcelo Z. Maialle* and Marcos H. Degani
Faculdade de Ciências Aplicadas, Universidade Estadual de Campinas-UNICAMP, R. Pedro Zaccaria, 1300, 13484-350 Limeira, São Paulo, Brazil

(Received 30 December 2010; published 11 April 2011)

We present results from numerical simulations of the photocurrent generated by intersubband optical transitions in a double quantum well coupled with a continuum of extended states. The photocurrent spectra are obtained directly from the time-dependent Schrödinger equation for the coherent regime without any adjusting parameters in the calculations other than the ones that define the physical system, also in a nonperturbative way and without basis-set expansions or truncations. A realistic representation of a three-level system in the Lambda ("Λ") configuration is investigated when two bound states in each quantum well are coupled by exciting fields via an excited quasibound state. Resonance between the exciting fields and the quantum states leads to coherent effects such as Rabi-dressed states, electromagnetically induced transparency, and population trapping, which are investigated in terms of the photocurrent spectral changes; that is, the coherent optical dynamics can be seen from the photocurrent signal. An excitation scheme involving two-photon absorption was proposed to produce the population-trapping effects using only one exciting field.

DOI: 10.1103/PhysRevB.83.155308 PACS number(s): 78.67.De, 73.63.Hs, 42.50.Ar

I. INTRODUCTION

The process of optical excitation is often described by two-level systems driven by external fields.[1] Nowadays, with the advances in the growth of semiconductor structures, the coherent dynamics of the optical excitation has been experimentally observed with astonishing details[2–5] in solid-state systems. Semiconductor quantum dots and quantum wells are some of these systems due to their well-separated energy levels and improved optical qualities. Besides, they have a great advantage over similar optical systems, such as atomic or impurity level states, in which traditionally the coherent optical excitation has been investigated, since their optoelectronic properties can be tailored by structural design.

Not only the two-level systems are good models for the coherent optical excitation dynamics, but other few-level systems have fulfilled the role, especially when the dynamics investigated has nonlinear behavior, such as happens in intense excitation regimes.[6] As common examples are the models of three-level systems in vee ("V") or Lambda ("Λ") configurations, which show a very rich dynamics when multiresonances are set in. Very often, photonic cavities enclosing the semiconductor few-level system contribute in the investigations by improving both frequency selection and intensity enhancement of the exciting fields.[7] Optical cavity fields have also been used to couple spatially separated quantum dots.[8]

A very common theoretical framework to deal with these multilevel systems is based on the solutions of the optical Bloch equation for the density matrices, $i\hbar\frac{d\rho}{dt} = [H,\rho] +$ decay terms.[1,9] The density-matrix components give both the occupation (diagonal) terms and the coherence (off-diagonal) terms, and different decay mechanisms can be incorporated as well. However, a weakness in this framework is in the limitation of the number of states accounted for usually motivated from practical reasons.

In realistic systems, as the quantum dots and wells mentioned above, the ground state is usually taken as the vacuum state $|0\rangle$ and the excited states are excitonic states, that is, Coulomb bound electron-hole pairs. Many-exciton complexes (e.g., biexcitons) or charged excitons (e.g., trions) can also be treated as excited states in these multilevel models. Experiments in strain-free quantum dots have recently addressed these exciton complexes.[10] Multilevel systems are equally well suitable to treat intersubband (intraband) transitions, for instance, as those between adjacent quantized energy states in the conduction band of semiconductor quantum dots or quantum wells. For intersubband transitions, due to the proximity in energy of the states (typically a few tens of meV), the excitation must be in the range of infrared radiation or terahertz oscillating fields. This has been a challenge, in comparison with the optical excitations in the interband (valence-to-conduction band) transitions, mainly due to the difficulty of generating and manipulating these lower-frequency waves. Nonetheless, progress has been made and the coherent dynamics in intersubband transitions has been observed.[11]

In the present work we have investigated the excitation dynamics within the subband structure of a realistic system without relying on few-level models. Instead, we have calculated directly from the time-dependent Schrödinger equation for the wave functions the excitation from the fundamental state to excited states. The exciting field was taken as a classical oscillating electric field whose frequency was controlled to allow spectral resolution in the energy-absorbing dynamics. The photocurrent was calculated as a response signal to access the dynamics. The coupling of the excited states with the continuum of extended states generates the current, and the same coupling also plays the role of a decaying channel for the occupation of the excited states. Additionally, a pair of exciting fields was used to introduce coupling of bound states spatially apart, and coherent population trapping, Rabi-dressed states, and electromagnetically induced transparency could be observed in the photocurrent signal. Although our simulations could tailor the time dependence of the exciting fields, we preferred to focus primarily on the spectral analysis of the effects hoping to furnish new elements and motivate further experimental studies which are easily done in frequency

domain. It was found that the photocurrent spectra present anticrossings associated with the strongly driven resonances, and since our treatment was nonperturbative, we were able to simulate a new proposal for attaining population trapping using only one exciting field.

II. THEORY

The system investigated is depicted in Fig. 1(a). It consists of a double quantum well having at its left-hand side a potential barrier to avoid electron current directed toward the left, and at the right-hand side there is a continuum of extended states separated by a thin potential barrier from the wells. Similar systems were investigated both theoretically[12] and experimentally[13] from the optical-property point of view.

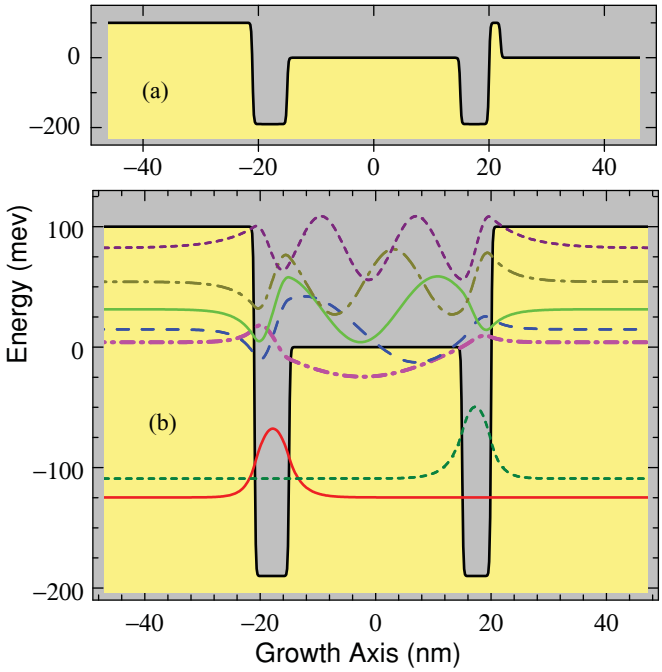

i	Ei (meV)	Ei-E1 (meV)	Ei-E2 (meV)	<i|x|1> (nm)	<i|x|2> (nm)
1	-124.75	0	-15.66	-17.72	0.002
2	-109.10	15.66	0	0.002	17.18
3	3.97	128.73	113.07	-0.77	0.38
4	14.74	139.49	123.84	1.19	0.66
5	31.40	156.16	140.50	1.03	-0.89
6	54.25	179.00	163.35	0.65	1.00
7	82.20	206.96	191.30	-0.38	0.83

FIG. 1. (Color online) (a) Schematics of the double quantum well investigated. The potential barrier at the left and the thin (2 nm) barrier at the right-hand side are at 100 meV, the wells (left 6-nm-, right 5-nm-wide) are at −190 meV, the barrier (30 nm) between the wells and the continuum at the right-hand side are at 0 meV. (b) System with an additional potential barrier on the right-hand side showing seven bound states $|i\rangle$, $i = 1,\ldots,7$. The table at the bottom shows the energies, transition energies, and dipole moment of the transitions. Eigenstates were calculated numerically using the split-operator method with imaginary-time propagation, as detailed in Ref. 16.

They are also similar to structures proposed to work as infrared photodetector (QWIP),[14] therefore specially designed to generate photocurrent.[15] The material's parameters are taken from GaAs, with the electron effective mass $m = 0.067m_0$, m_0 being the free electron mass. The energy offsets are shown in the caption of Fig. 1 and they can be set as in GaAs/Al_xGa_{1-x}As structures for Al concentration on the order of 30%. If we replace the continuum at the right by a barrier similar to the one at the left, the system exhibits seven bound states, two of them localized in each well [states $|1\rangle$ and $|2\rangle$ in Fig. 1(b)]. The states $|3\rangle$ to $|7\rangle$ become quasibound states when the continuum is reconsidered into the system as in Fig. 1(a). Nonetheless, states $|3\rangle$ to $|7\rangle$ give us an idea of which energy levels are more strongly coupled with the continuum. The table at the bottom of Fig. 1 gives the eigenenergies for the system in Fig. 1(b), as well as the transition energies and the dipole moments $\langle i|x|j\rangle = \int \psi_i^*(x)x\psi_j(x)dx$. These moments give the coupling strength between the states $|i\rangle$ and $|j\rangle$ by an electric field oscillating along the system axis (x direction). Note the very small coupling between the states $|1\rangle$ and $|2\rangle$ ($\langle 1|x|2\rangle = 0.002$ nm) as a result of the large separation between the wells (30 nm). On the other hand, states $|1\rangle$ and $|2\rangle$ show a much larger degree of coupling with the excited states $|3\rangle$ to $|7\rangle$.

Within the effective-mass approximation for a one-electron problem in the conduction band, the following one-dimensional Hamiltonian is used:

$$H = -\frac{\hbar^2}{2m}\frac{d^2}{dx^2} + V(x) - exF_1\sin(\Omega_1 t) - exF_2\sin(\Omega_2 t), \quad (1)$$

where the electron effective mass m is taken as uniform throughout the system, $V(x)$ is the potential due to the material band offsets, and F_1 (F_2) is the amplitude of the applied electric field oscillating with frequency Ω_1 (Ω_2).

The ground state of the system in Fig. 1(a) is calculated within a split-operator method[16] first without the application of exciting fields, and it is used as the initial state $\Psi(x,0) = \langle x|1\rangle$ to be advanced in time under the full Hamiltonian [Eq. (1)]. For an infinitesimal time increment Δt, the time evolution can be obtained from

$$\Psi(x,t+\Delta t) = e^{-iH\Delta t/\hbar}\Psi(x,t). \quad (2)$$

Since such operation cannot be done exactly, approximations are needed to evolve the wave function, and we have used

$$e^{-i(T+V)\Delta t/\hbar} = e^{-iV\Delta t/2\hbar}e^{-iT\Delta t/\hbar}e^{-iV\Delta t/2\hbar} + O(\Delta t^3), \quad (3)$$

where T and V are, respectively, the kinetic and potential (including the electric field terms) operators shown in the Hamiltonian [Eq. (1)]. Equation (3) is a unitary operation which gives stability to the method within an error of order $O(\Delta t^3)$. Successive applications of this procedure can evolve the initial wave function to a given time t. Details of the numerical procedure are given in Ref. 16.

Under the action of the exciting field, the initial state $\Psi(x,0)$ can be excited in energy and it can couple with the continuum, mainly via the quasibound states $|3\rangle$ to $|7\rangle$, to create a particle current flowing toward both sides of the structure. The barrier located at the left-hand side favors most of the current to be directed toward the right for the excitation energies (i.e., field

frequencies Ω) used. It is important to stress the fact that the states $|i\rangle$, $i = 2,\ldots,7$, calculated and shown in Fig. 1(b) are *not* used in our analysis. Only the time evolution of one state, $\Psi(x,t)$, is needed.

The current is calculated[15] at given points $x_c = x_L$ (x_R) in the left(right)-hand side region by the expression

$$J_c(t) = \Re\left(\frac{\hbar}{im}\Psi(x,t)^*\frac{\partial\Psi(x,t)}{\partial x}\right)\Bigg|_{x=x_c}, \tag{4}$$

with $c = L$ or R, from which the integrated current is obtained

$$I = \int_0^T [J_R(t) - J_L(t)]dt. \tag{5}$$

From now on we refer to this current as "photocurrent," which is calculated as a function of the excitation energy (i.e., field frequency Ω), yielding the photocurrent spectra we discuss in the remainder of this work.

Our numerical method utilizes hard-wall boundary conditions; that is, the wave functions vanish at the boundaries of the system.[16] This causes reflections at the boundaries and produces interference effects in the current. We have employed exponential imaginary-potential barriers[17] in the boundary regions in order to minimize current reflections.[18]

III. RESULTS AND DISCUSSION

A. One-field photocurrent spectra

The photocurrent spectrum in Fig. 2(a) shows a series of peaks for the transitions starting in the initial state $|1\rangle$, being enhanced by the quasibound states $|i\rangle$, $i = 3,\ldots,7$, and tunneling to the continuum. The bound state $|2\rangle$, localized in the narrower quantum well at the right, does not participate since its dipole element with the initial state is very small (cf. Fig. 1). The energy positions of the peaks in Fig. 2(a) agree well with the transition energies shown in the table of Fig. 1. Besides, higher energy peaks appear broader as one would expect due to their shorter lifetimes (stronger coupling with the continuum). This can be better seen in Fig. 2(b), which shows the same graph but now in logarithm scale.

A technical point should be discussed here. In Eq. (5), the current $J(t)$ is integrated in time from $t = 0$ to a certain upper limit $t = T$. Since the system is initialized with one electron occupying the state $|1\rangle$, and the action of the oscillating field is accumulative in time, for very long times the state can be completely ionized such that I achieves an upper bound value, no longer dependent on T. However, this limiting case occurs at different times for different excitation energies in the photocurrent spectra, since each excitation energy has a given coupling strength between the states involved in the transition. The amplitude F_1 of the exciting field also plays a similar role, since stronger fields ionize faster the initial state. We therefore have to decide which value of T to use for all excitation energies, for a given field amplitude, when computing the photocurrent spectra.

In Fig. 2(d) it is shown the photocurrent peak maximum for the transition 1–4 as function of the field amplitude, fixing $T = 13$ ps (Note that this value for T is much larger than the oscillating field period, which is about 30 fs for transition energies around $\hbar\Omega \sim 150$ meV. Also, the time step in the

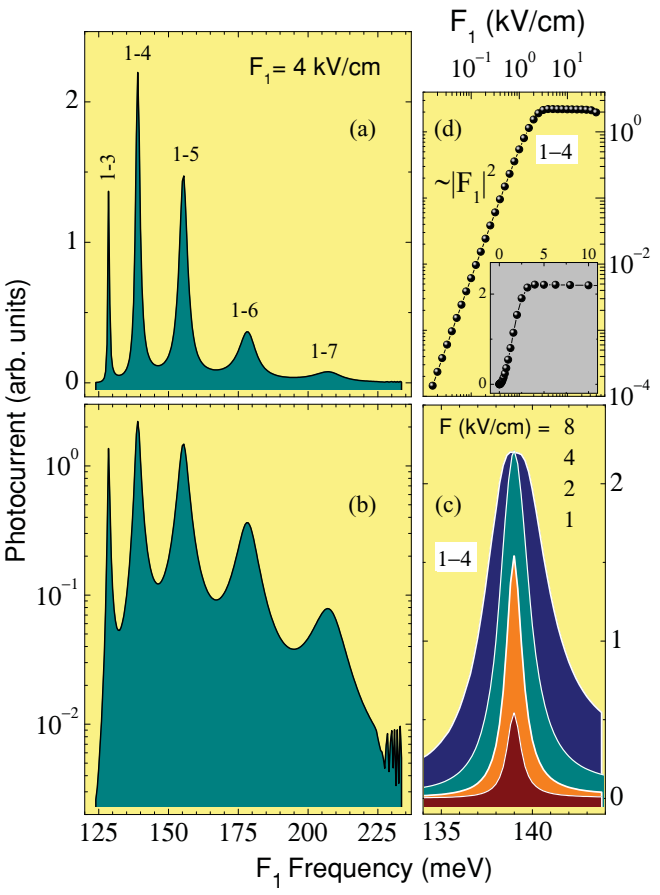

FIG. 2. (Color online) (a) Field-induced current (photocurrent) as function of the exciting field frequency (energy $= \hbar\Omega_1$) for a field amplitude of 4 kV/cm. Peak labels 1–n indicate transitions from the initially occupied state $|1\rangle$ to the final quasibound state $|n\rangle$. (b) The same as in (a) but in logarithm scale. (c) Photocurrent peak 1–4 for different amplitude of exciting field showing saturation effects. (d) Peak 1–4 maximum (in log scale) as function of field amplitude. The inset shows the same in linear scale.

numerical simulations is 0.8 fs. It can be seen from the log scale a quadratic dependence of the current peak with the field amplitude, for F_1 lower than ∼3 kV/cm, which corresponds to a linear dependence of the photocurrent with the field intensity (power). However, for F_1 larger than 3 kV/cm, there is a saturation of the peak maximum indicating complete ionization (in fact, there is additionally some Rabi oscillation contributing to this saturation, which will be discussed in connection with Fig. 3). We decided to set the value of T, for a given field amplitude F_1, such that the strongest peak in the spectrum just starts to show saturation (i.e., complete ionization). In the case of Figs. 2(a) and 2(b), $F_1 = 4$ kV/cm and $T = 13$ ps were used. In Fig. 2(c) it is shown the saturation effect on the peak 1–4 for $T = 13$ ps and increasing values of F_1. Notice that, as the peak saturates with increasing field amplitude, the transitions on the shoulders of the peak follow the same trend, resulting in the broadening of the whole spectrum. We better avoid this "spurious" broadening by controlling T and F_1. This saturation-induced broadening can be considered spurious in specific experimental situations in which the initial state $|1\rangle$ is always occupied by electrons

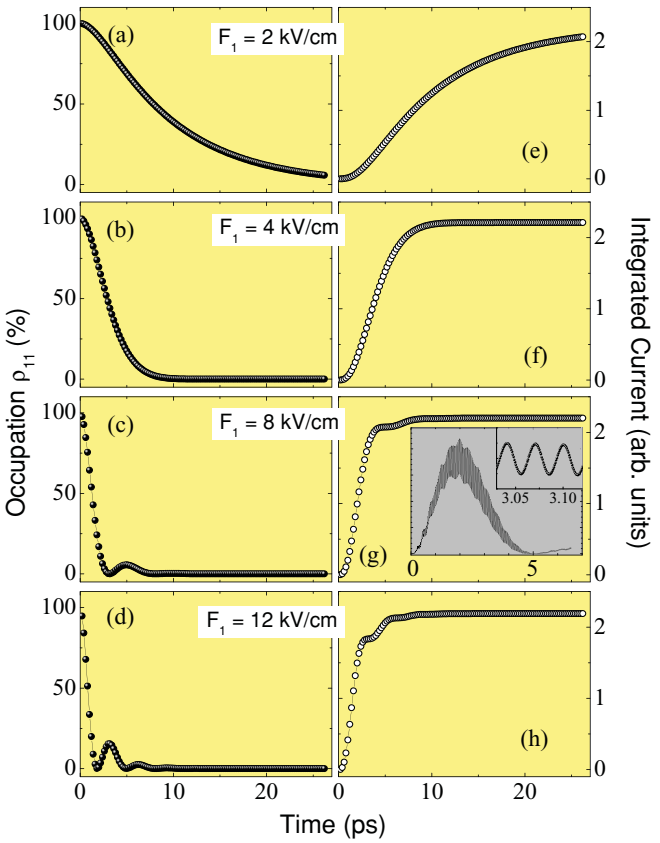

FIG. 3. (Color online) Time dependences calculated at the resonant condition for the transition between the initial state $|1\rangle$ and the quasibound state $|4\rangle$. (a)–(d) Occupation of the initial state, as defined in Eq. (6), and (e)–(h) time-integrated current $I(T)$, as in Eq. (5), as functions of time for different intensities of the exciting field. The inset shows the current $J(t)$, defined in Eq. (4), whose integral $I(T) = \int_0^T J(t)dt$ yields (g). The fast oscillation in $J(t)$ is amplified in the upper part of the inset showing the current response to the exciting field oscillation at a period of about 30 fs.

given by some charge source, such as doping impurities, in which case the saturation discussed here for the photocurrent is not so easily achieved.

The spectra shown in Fig. 2 are the photocurrent integrated in time according to Eq. (5). It is interesting to see the time dependence which was hidden by the integration, and this is shown in Fig. 3. In Figs. 3(a), 3(b), 3(c), and 3(d), the occupation of the initial state $|1\rangle$ as function of time is shown for different amplitudes of the exciting field F_1. The occupation is defined as the probability of finding the system state, at time t, in the initial state $\langle x|1\rangle = \phi_1(x)$; that is,

$$\rho_{11}(t) = \left| \int \phi_1^*(x)\Psi(x,t)\,dx \right|^2 . \qquad (6)$$

In these panels we observe the initial occupation decaying as result of the ionization by the oscillating field, yielding the photocurrent $J(t)$, whose integral $I(T) = \int_0^T J(t)dt$ is shown on the panels at the right-hand side [Figs. 3(e), 3(f), 3(g), and 3(h)] as a function of T. For increasing field amplitudes the decay of ρ_{11} is more accentuated. For the intensities $F_1 =$ 8 and 12 kV/cm, ρ_{11} oscillates since the states $|1\rangle$ and $|4\rangle$ become coherently coupled by the exciting field. These are the Rabi oscillations which in the present case are damped by the tunneling of the initially bound state to the continuum. In Fig. 2 we have used $T = 13$ ps and $F_1 = 4$ kV/cm and note that this value of T is the one in which the initial state just ionizes [Fig. 3(b)] and the current I saturates [Fig. 3(f)].

An interesting fact is that the Rabi oscillations seen in the time evolutions of Fig. 3 have not given any signature on the photocurrent spectrum, as we can see, for example, in Fig. 2(c) for increasing field amplitude. Rabi oscillations can give a doublet in the absorption or transmission spectra with peaks separated by the Rabi frequency $\Omega_R = \mu F_1/\hbar$ (μ as the dipole moment), but no splitting of the photocurrent peaks were observed. In reality, only a small contribution to the saturation of I had to do with the Rabi oscillations, which was, however, hidden by the faster ionization. In an experimental condition with many electrons in the initial state, as already mentioned, possibly given by doping, this saturation can be obscured and not observed. Nonetheless, Rabi oscillations were already measured in photocurrents for a single quantum dot in a photodiode.[4] In this case, the photocurrent oscillated for increasing amplitude of the exciting field, which was pulsed in time (1 ps width): Every time the amplitude matched the π-pulse condition (complete inversion of the two-level system) the photocurrent attained a maximum value. For our simulation, the strong coupling to the continuum is causing a fast decay of the initial state and it is preventing the observation of similar effect for increasing field intensities. Notice that we could simulate a case in which the decay rate to the continuum would be weaker just by making the potential barrier at the right-hand side of the system [see Fig. 1(a)] thicker as we wish. Also, we could adjust the time duration of the exciting field to produce any desirable condition, such as π pulses. Instead of investigating these degrees of freedom in the time domain, as we have pointed out in the Introduction, we preferred to simulate a cw excitation condition (i.e., long-lived exciting field) and explored the frequency domain changes introduced by the coherent excitation dynamics in the photocurrent spectra.

B. Two-field photocurrent spectra

The use of a second exciting field creates new and richer excitation dynamics for the system investigated. So far, with only one exciting field, we were basically field driven a two-level system which had an excited state coupled with the continuum. This coupling had a dual role since it introduced a decaying rate and it allowed for the generation of photocurrent which was our response signal for the dynamics. The bound state localized in the right-hand side well, state $|2\rangle$, has not participated in the dynamics so far. A second exciting field can be used to drive this state. By choosing the frequencies of the two exciting fields properly, we can set a condition for a three-level system in the Λ configuration, that is, the coupling between the states $|1\rangle$ and $|2\rangle$ can be done by the two fields via an intermediary excited state, for instance, one of the quasibound states $|i\rangle$, with $i = 3, \ldots, 7$.

Two-field spectroscopy has been successfully used to investigate strongly driven single quantum dots,[2] in which Rabi oscillations had an effect.[19] In this study, the quantum dot

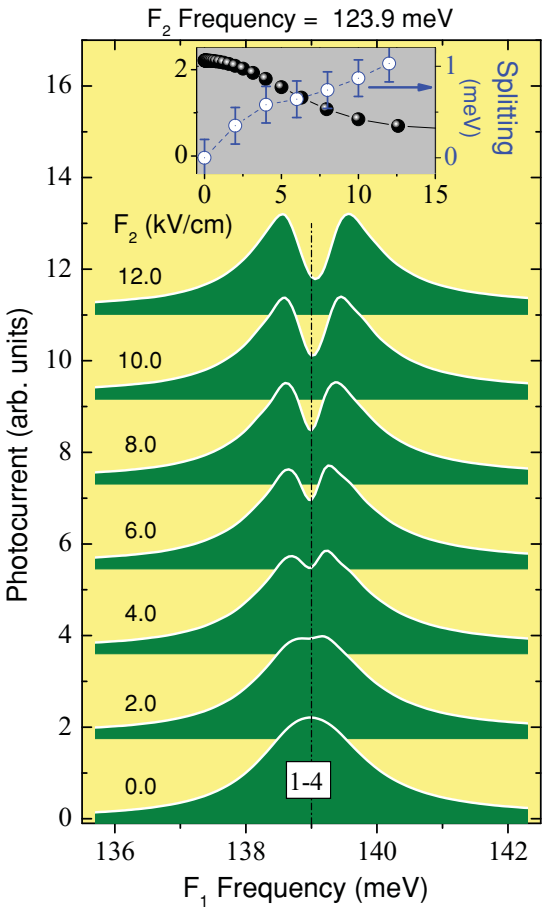

FIG. 4. (Color online) Photocurrent spectra focused at the 1–4 transition peak, with exciting field amplitude $F_1 = 4\,\mathrm{kV/cm}$, showing the effect of a second field with different amplitudes F_2 and resonant with the 2–4 transition ($\hbar\Omega_2 = 123.9$ meV). Spectra are shifted vertically for better visualization. The inset shows (open symbols with error bars) the energy splitting as function of the amplitude F_2 and (solid symbols) the photocurrent calculated at the resonant frequency for the transition 1–4 (139 meV) as it is shown by the vertical dotted line in the spectra.

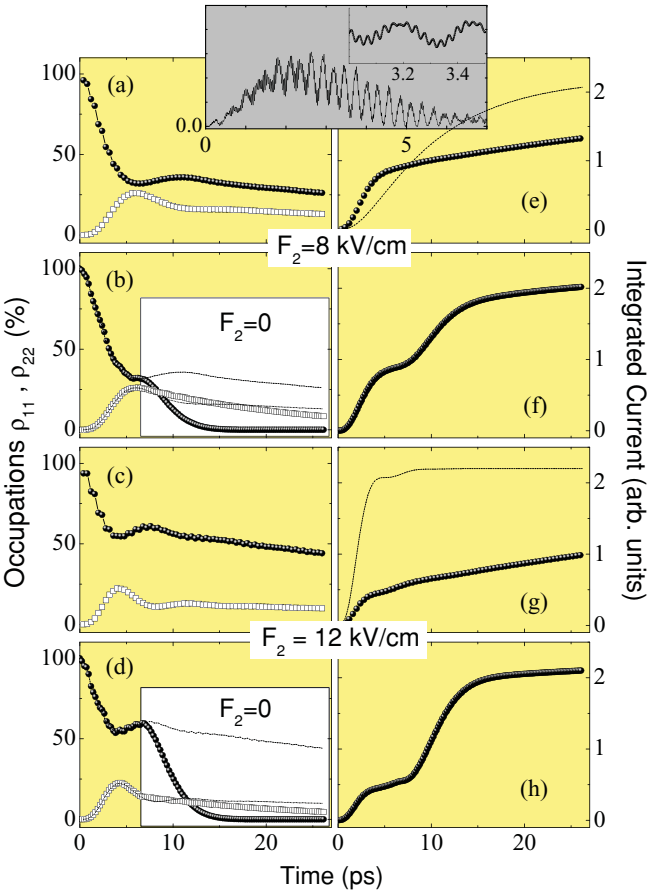

FIG. 5. (Color online) Time dependences calculated at the resonant condition for the transition 1–4 and with a field amplitude $F_1 = 4\,\mathrm{kV/cm}$. A second field of amplitude F_2 excites the transition 2–4 in resonance. (a)–(d) Occupation of the initial state ρ_{11} (solid symbols) and the first excited state ρ_{22} (open symbols), as defined in Eq. (6), and (e)–(h) time-integrated current $I(T)$, as in Eq. (5), as functions of time for different intensities of the exciting field F_2. In (b) and (d), the second field amplitude F_2 vanishes within the white box area in the graph. In (e) and (g) the lines are the photocurrent $I(T)$ without the second field (i.e., $F_2 = 0$) as shown before in Figs. 3(g) and 3(h). The inset shows the current $J(t)$ whose integral gives $I(T) = \int_0^T J(t)dt$ shown in (e). The fast oscillation in $J(t)$ is amplified in the upper part of the inset showing the current response to the exciting field oscillation at a period of ∼30 fs and a beating period of ∼250 fs due to the action of two exciting fields.

behaved as a three-level system in a V configuration, and while one of the pair of transitions was strongly driven by a resonant field, the other transition was spectrally resolved by optical absorption. This is the situation for which the Autler-Towners doublet appears. Additionally, the Mollow triplet was also seen when the same transition of the V-like system was strongly driven and simultaneously spectrally resolved. We can use similar approach in our Λ-like system to investigate the Rabi oscillation effects on the photocurrent signal.

In Fig. 4 the two-field spectra are shown with a second field tuned at the resonance energy ($\hbar\Omega_2 = 123.9$ meV) coupling the states $|2\rangle$ and $|4\rangle$. Note that this energy is sufficiently low to prevent the excitation of the transitions from the initially occupied state $|1\rangle$ to any state in the continuum (one would need at least 124.75 meV to excite the continuum directly and 128.73 meV to excite the first quasibound state $|3\rangle$). Therefore, this second field alone does not produce photocurrent from the initial state $|1\rangle$ in the low excitation regime (we see below that higher excitation intensities yield nonlinear absorption, but not specifically in this energy range). In Fig. 4 the amplitude F_2 is varied from zero to 12 kV/cm and the other field, with amplitude $F_1 = 4\,\mathrm{kV/cm}$, is used to scan across the transitions 1–4. It is seen from the spectra in Fig. 4 that, for increasing F_2, the peak 1–4 splits in a doublet and that the energy splitting is proportional to F_2 as shown in the inset. The explanation for this splitting is the same as the one given in Ref. 2, that is, the field F_2 dressed the transition 2–4 causing a Rabi doublet. The field F_1 then couples the initial state $|1\rangle$ with the Rabi-splitted state $|4\rangle \rightarrow (|4'\rangle, |4''\rangle)$.

The effects of the second field, in resonance with the 2–4 transition, can be seen in a different way besides the dressed-state interpretation given above. The Λ system, when excited by two fields in resonance (in our case, for example, resonant

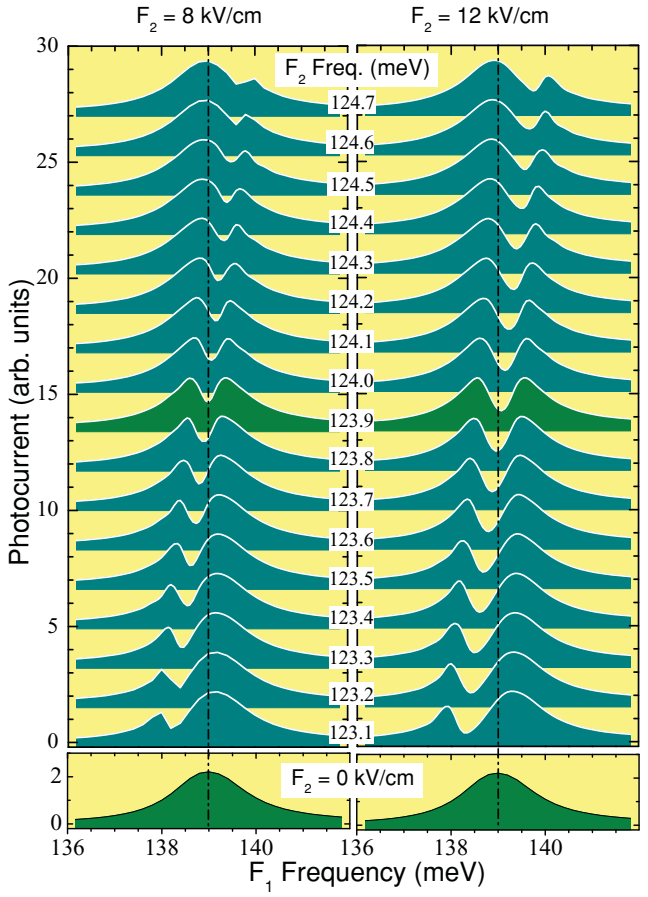

FIG. 6. (Color online) Photocurrent spectra focused at the peak transition 1–4 in the presence of two exciting fields. One field has amplitude $F_1 = 4$ kV/cm, and the other is $F_2 = 8$ kV/cm (left panel) and 12 kV/cm (right panel). Spectra are shifted vertically for different frequencies Ω_2 of the field exciting the 2–4 transition. $\hbar\Omega_2 = 123.9$ meV sets the 2–4 resonance. At the bottom are the spectra for the 1–4 peak with only one field acting. The vertical dotted lines are guide to the eyes indicating the 1–4 resonance.

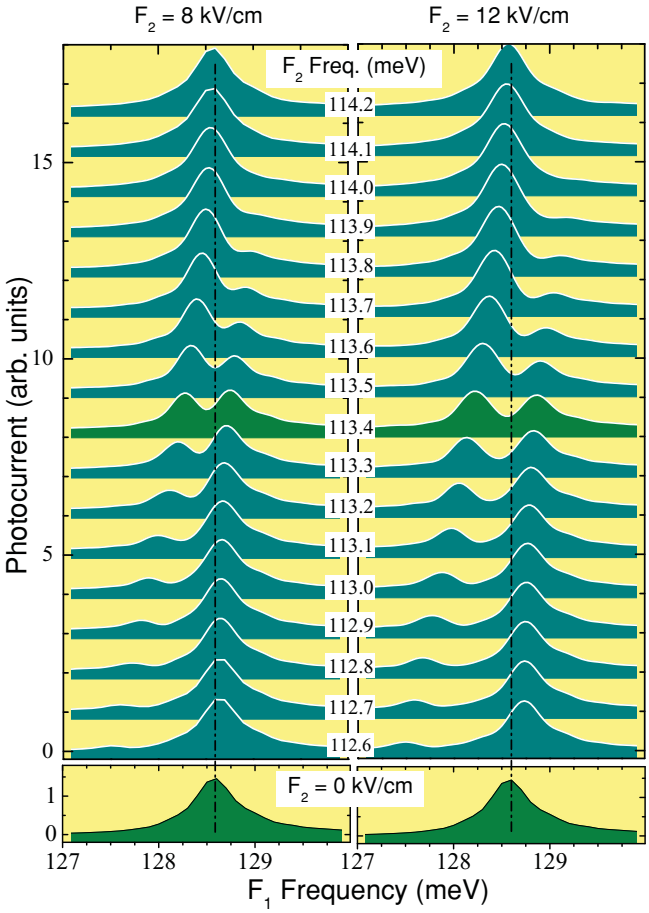

FIG. 7. (Color online) The same as in Fig. 6, now in the energy range involving the excited quasibound state $|3\rangle$ instead of $|4\rangle$.

with the transitions 1–4 and 2–4) can produce the so-called "coherent population trapping."[6] This effect is a coherent excitation coupling of the bound states $|1\rangle$ and $|2\rangle$ through an excited state, for example, $|4\rangle$. A characteristic of this situation is that the occupation of the excited state is null, that is, $\rho_{44} = 0$. This also leads to the well-known "electromagnetically induced transparency."[20] In our system this means vanishing photocurrent. The decrease in the photocurrent signal at the transition energy 1–4 (dotted line in Fig. 4) is a signature of such effect in the spectral domain. In fact, the inset (solid points) in Fig. 4 shows a photocurrent decrease as a function of the amplitude F_2. In order to see the population trapping in the time domain, Fig. 5 gives the occupations of the states $|1\rangle$ and $|2\rangle$ as functions of time. It is observed that now, besides ρ_{11}, also ρ_{22} is excited. The population trapping is revealed by the suppression of the occupations' decaying in time due to the lack of tunneling to the continuum (lack of photocurrent). In Figs. 5(b) and 5(d) the second field is vanished after 6.5 ps, allowing the photocurrent to resume [cf. Figs. 5(f) and 5(h)] but leaving behind a finite occupation of state $|2\rangle$. Note that a partial coherent population transfer is accomplished between states $|1\rangle$ and $|2\rangle$, which are well spatially separated, with very little overlap and small dipole moment between them.

It is also interesting to see the behavior of the peak 1–4, when it is split by the presence of a second field F_2, with the latter field being detuned from the resonance 2–4. This is shown in Fig. 6 for two amplitudes $F_2 = 8$ and 12 kV/cm, while $F_1 = 4$ kV/cm. For comparison, at the bottom of Fig. 6, the photocurrent peak 1–4 is shown for the case of only one field (i.e., $F_2 = 0$). It is observed that as $\hbar\Omega_2$ scans across the transition 2–4, the splitting remains even in the resonant condition $\hbar\Omega_2 = 123.9$ meV. In fact, an anticrossing pattern is clearly observed.

Everything we have discussed for the transitions involving the quasibound state $|4\rangle$ can potentially happen to any other excited state, which together with $|1\rangle$ and $|2\rangle$ constitute a Λ system. For example, in Fig. 7 the excited quasibound state $|3\rangle$ is investigated, yielding a similar situation as given before in Fig. 6 when state $|4\rangle$ was involved.

C. Two-photon, one-field population trapping

The population trapping effect investigated so far relied in the condition of having two exciting fields in resonance with the two transitions of the Λ system. This is a two-color excitation scheme. It would be interesting to obtain such effect with only one exciting field (one-color scheme). To accomplish

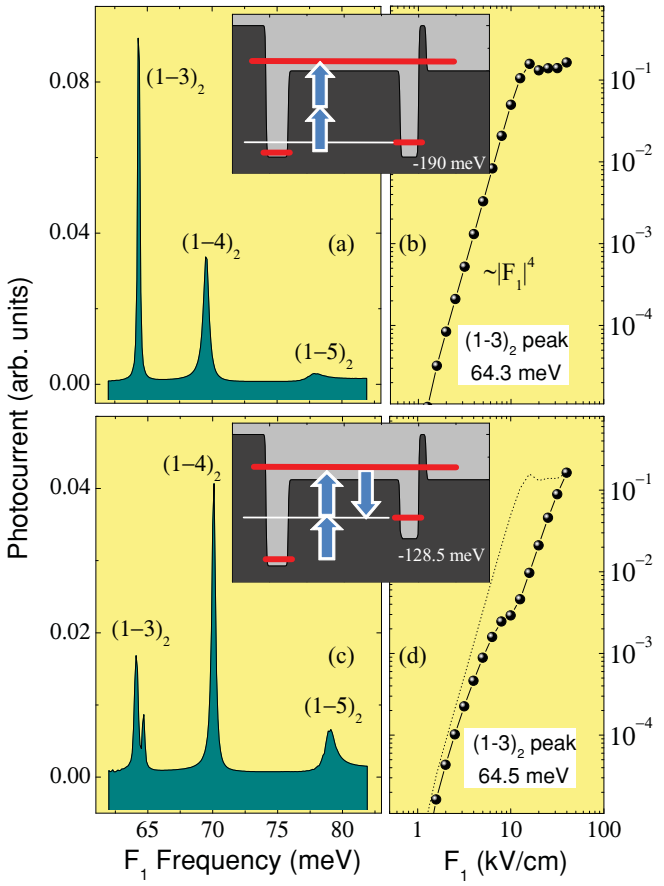

FIG. 8. (Color online) (a),(c) Photocurrent spectra for the systems shown in the insets under nonlinear absorption ("two-photon" process). The peaks in the spectra are labeled according to the initial and final states: $(1-n)_2$, with $n = 3$, 4, and 5. The exciting field amplitude is $F_1 = 12$ kV/cm. (b),(d) Photocurrent peak intensity, in log scale, for the transition $(1–3)_2$ as a function of the field amplitude F_1.

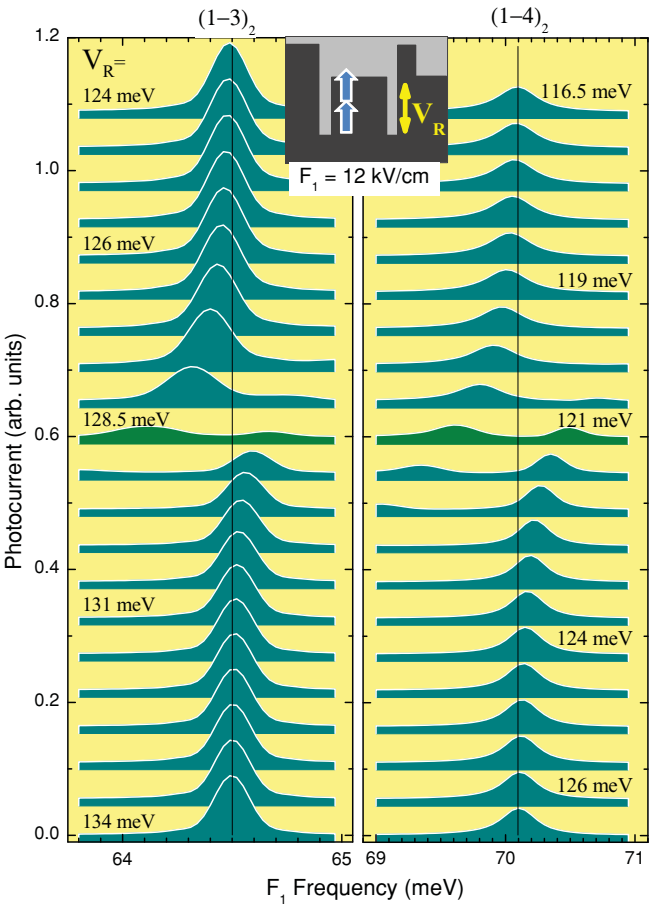

FIG. 9. (Color online) Photocurrent spectra for the system proposed in Fig. 8 for different values of the potential V_R for the narrower quantum well at the system right-hand side. Left-hand side panels are for near resonance with the transition $(1–3)_2$, and right-hand side panels are similar ones for the transition $(1–4)_2$. The intensity of the exciting field is $F_1 = 12$ kV/cm.

that, both transitions in the Λ system have to be excited in resonance, simultaneously, by only one field. One possibility is the case in which both transitions have the same energy (we could call it "symmetric Λ system"). This implies the lower-energy states $|1\rangle$ and $|2\rangle$ to be degenerate, and that may raise a question about which one of the states is initially occupied. On the contrary, an asymmetric system favors the ground (nondegenerate) state as the initially occupied state.

Even in the case of an asymmetric Λ system, there is an alternative scheme in which one could excite the upper state from the ground state by a two-photon absorption process and, with the same energy photon, connect the upper state with the first excited state [see the inset in Figs. 8(c) and 8(d)]. This scheme potentially produces a population trapping effect.

Since our simulation method does not rely on perturbative approaches, a two-photon transition can be naturally accounted for in our calculations. In Fig. 8(a) the photocurrent is calculated as before in Fig. 2, but now the exciting field frequency scans an energy range half of the necessary to promote the initial state $|1\rangle$ directly to the continuum. A series of peaks which are exactly at half of the energies shown for the series of peaks in Fig. 2(a) is found. Since these peaks are weaker, an increase in the exciting field amplitude is necessary (in Fig. 8, $F_1 = 12$ kV/cm, instead of 4 kV/cm used in Fig. 2). We attribute the existence of these peaks to a "two-photon" absorption process as depicted in the inset. The dependence shown in Fig. 8(b) of the photocurrent peak $(1–3)_2$ with the field amplitude is $\sim|F_1|^4$, that is, quadratic on the field intensity (power). This is consistent with a second-order transition process involving the absorption of two photons. As before in Fig. 2(d), a saturation effect appears at high excitation intensities due to the ionization of the initial state.

The present system [inset of Figs. 8(a) and 8(b)] does not excite the state $|2\rangle$ since it is off resonance. In order to set the resonance 2–3, the bottom of the right-hand side well is pushed up in energy from -190 meV in Fig. 8(a) to -128.5 meV, as shown in Fig. 8(c). In practice, this could be done by changing the composition of the material of the well in different samples, or even better, by applying a bias to control the energy levels in the same sample. Then the transition 2–3 becomes resonant with only one photon. Figure 8(c) presents the corresponding modification on the photocurrent spectra, in particular for the peak $(1–3)_2$, which now shows a decrease in the peak intensity and a splitting of the peak into a doublet. In Fig. 8(d) the

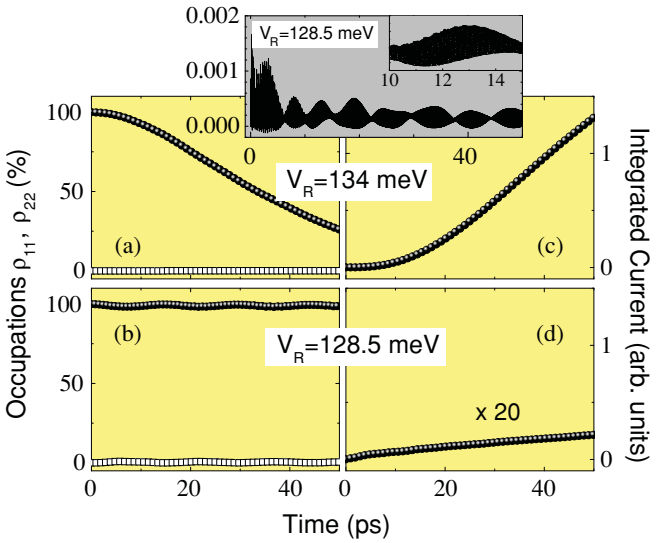

FIG. 10. (Color online) Time dependences of the energy level occupations ρ_{11} and ρ_{22}, for (a) off resonance and (b) on resonance conditions with respect to the transition $(1–3)_2$. (c) and (d) are, respectively, the corresponding integrated current $I(T) = \int_0^T J(t)dt$ as function of T. The inset shows the current $J(t)$, as a function of time t, in the resonant condition, showing beatings. An amplified view of $J(t)$ is also shown having the oscillatory behavior imposed by the exciting oscillatory field.

maximum of the peak $(1–3)_2$ is plotted as a function of the exciting field amplitude F_1, showing a strong decrease for the peak intensity in comparison with Fig. 8(b), besides a nontrivial dependence on F_1 which is no longer exactly $\sim|F_1|^4$.

The process of setting the transition 2–3 in resonance by changing the bottom of the right-hand side well (potential V_R) is shown by the set of spectra in Fig. 9. The left panel shows the effect on the photocurrent peak $(1–3)_2$, whereas the panel on the right shows the same for the peak $(1–4)_2$. Again, an anticrossing behavior is observed. At resonance [$V_R = 128.5$ meV for $(1–3)_2$ and $V_R = 121.0$ meV for $(1–4)_2$] the doublet observed has the same interpretation as that in Fig. 4, and they can be understood as a population trapping effect. The time dependences of the energy level occupations ρ_{11} and ρ_{22} are shown in Fig. 10 for the photocurrent peak $(1–3)_2$. In Fig. 10(a) V_R is set off resonance, while in Fig. 10(b) the resonant condition is satisfied (cf. Fig. 9). It is observed, in this case, that the decay of the occupation ρ_{11} is strongly suppressed, although the occupation ρ_{22} is not strongly increased.

IV. CONCLUSIONS

In conclusion, the current (called here photocurrent) generated by the effect of an oscillatory electric field on an initially occupied electronic state was calculated. The system investigated was an asymmetric double quantum well structure having excited energy levels coupled with a continuum of extended states. The simulations were done from the numerical solutions of the time-dependent Schrödinger equation, without any adjusting parameters other than the parameters defining the physical system, namely, the electron effective mass and the band-edge potential profile. In this respect, the present simulations are unique in solving the coherent excitation dynamics of a realistic semiconductor system, since in most of the previous works the investigation occurs under the simplified framework of few-level models. The dynamics extracted from these models often utilizes many matrix elements and relaxation/transition rates as inputs, which are obtained from auxiliary calculations. This was not needed in our model calculation based solely on the time evolution of a given initial state by the Schrödinger equation Eq. (1). The excitation dynamics shown by the photocurrent spectra presented many coherent effects usually investigated in the optical response, such as Rabi oscillations and splittings, population trapping, and electromagnetically induced transparency. It is interesting to compare the photocurrent spectra calculated here with the experimental optical absorption spectra of similar systems under similar excitation dynamics, such as for the quantum dot in Ref. 2. The photocurrent signal revealed basically the same effects as the optical response, which opens the possibility for obtaining information about the coherent excitation dynamics directly from the electronic signal. For that reason, we have intended to perform the simulations without manipulating the time degrees of freedom of the excitation process. Instead, our focus was on the spectral changes associated with the coherent excitation dynamics, which may be easier to be addressed experimentally in future works, such as in strongly driven infrared photodetectors, where many-photon absorptions were already shown to play an important role either via real[21] or virtual[22] intermediate states. The experimental challenges are, of course, enormous in order to realize a coherently excited photodetector. Nonetheless, the present model is well suitable to describe the coherent excitation dynamics especially in systems having a continuum of states, as the system we investigated, and as for the systems used for infrared photodetector devices (QWIP or QDIP).[14] In fact, our model was recently extended to treat a three-dimensional system, namely, a quantum dot coupled with both a quantum well and a continuum, and the simulation could describe quite well the photocurrent data involving sequential photon absorptions.[23]

ACKNOWLEDGMENTS

The authors acknowledge financial support from DISSE-Instituto Nacional de Ciência e Tecnologia de Nanodispositivos Semicondutores and CNPq-Conselho Nacional de Desenvolvimento Científico e Tecnológico, Brazil. M.Z.M. is grateful to J. M. Villas-Bôas for many useful discussions and suggestions.

*marcelo.maialle@fca.unicamp.br

[1] L. Allen and J. H. Eberly, *Optical Resonance and Two Level Atoms* (Wiley, New York, 1975).

[2] Xiaodong Xu, Bo Sun, P. R. Berman, D. G. Steel, A. S. Bracker, D. Gammon, and L. J. Sham, Science **317**, 929 (2007).

[3]B. D. Gerardot, D. Brunner, P. A. Dalgarno, K. Karrai, A. Badolato, P. M. Petroff, and R. J. Warburton, New J. Phys. **11**, 013028 (2009).
[4]A. Zrenner, E. Beham, S. Stufler, F. Findeis, M. Bichler, and G. Abstreiter, Nature (London) **418**, 612 (2002).
[5]H. Htoon, T. Takagahara, D. Kulik, O. Baklenov, A. L. Holmes Jr., and C. K. Shih, Phys. Rev. Lett. **88**, 087401 (2002).
[6]Z. Ficek and S. Swain, in *Quantum Interference and Coherence: Theory and Experiment*, Springer Series in Optical Sciences, Vol. 100 (Springer, Berlin, 2005), Chap. 5.
[7]K. Hennessy, A. Badolato, M. Winger, D. Gerace, M. Atatüre, S. Gulde, S. Fält, E. L. Hu, and A. Imamoglu, Nature (London) **445**, 896 (2007).
[8]A. Laucht, J. M. Villas-Bôas, S. Stobbe, N. Hauke, F. Hofbauer, G. Böhm, P. Lodahl, M.-C. Amann, M. Kaniber, and J. J. Finley, Phys. Rev. B **82**, 075305 (2010).
[9]S. Mukamel, *Principles of Nonlinear Optics and Spectroscopy* (Oxford University Press, New York, 1995).
[10]M. Abbarchi, T. Kuroda, T. Mano, K. Sakoda, C. A. Mastrandrea, A. Vinattieri, M. Gurioli, and T. Tsuchiya, Phys. Rev. B **82**, 201301(R) (2010).
[11]E. Dupont, H. C. Liu, A. J. SpringThorpe, W. Lai, and M. Extavour, Phys. Rev. B **68**, 245320 (2003).
[12]Jin-Hui Wu, Jin-Yue Gao, Ji-Hua Xu, L. Silvestri, M. Artoni, G. C. La Rocca, and F. Bassani, Phys. Rev. Lett. **95**, 057401 (2005).
[13]J. Faist, F. Capasso, C. Sirtori, K. W. West, and L. N. Pfeiffer, Nature (London) **390**, 589 (1997).
[14]B. F. Levine, J. Appl. Phys. **74**, R1(8) (1993).
[15]M. Z. Maialle, M. H. Degani, J. R. Madureira, and P. F. Farinas, J. Appl. Phys. **106**, 123703 (2009).
[16]M. H. Degani and M. Z. Maialle, J. Comput. Theor. Nanosci. **7**, 454 (2010).
[17]Á. Vibók and G. G. Balint-Kurti, J. Phys. Chem. **96**, 8712 (1992).
[18]D. Neuhasuer and M. Baer, J. Chem. Phys. **90**, 4351 (1989).
[19]A. J. Ramsay, Semicond. Sci. Technol. **25**, 103001 (2010).
[20]K.-J. Boller, A. Imamoglu, and S. E. Harris, Phys. Rev. Lett. **66**, 2593 (1991).
[21]H. Schneider, H. C. Liu, S. Winnerl, C. Y. Song, O. Drachenko, M. Walther, J. Faist, and M. Helm, Infrared Phys. Technol. **52**, 419 (2009).
[22]A. Zavriyev, E. Dupont, P. B. Corkum, H. C. Liu, and Z. Biglov, Opt. Lett. **20**, 1885 (1995).
[23]M. H. Degani, M. Z. Maialle, P. F. Farinas, N. Studart, M. P. Pires, and P. L. Souza, J. Appl. Phys. **109**, 064510 (2011).